RSC Advances

PAPER

View Article Online
View Journal | View Issue

Cite this: *RSC Adv.*, 2026, **16**, 27048

The geometric role of the time parameter in DNA base-pair genetic information exchange and assembly: applications of Frenet–Serret formulas to circular and elliptical helix models

May-Ru Chen, *[a] Wilson Agerico Diño, [b] Federico Palazzetti[c] and Toshio Kasai*[bd]

This study employs tools from differential geometry to quantitatively reexamine the relationship between the chemical structure of biomacromolecules, such as DNA, and their geometric organization relevant to genetic information storage. We introduce the concept of an action-time parameter, *t*, and its correlation with the arclength, *s*, of three-dimensional curves, as exemplified by the canonical double helix, to provide a geometric framework for assessing the robustness of structural descriptors commonly used in chemical and biochemical studies of DNA. Using the Frenet–Serret formulas, we demonstrate a clear linear relationship between *t* and *s*. This highlights a consistent geometric parametrization of molecular structure. The invariance of curvature and torsion under geodesic curve conditions is a key geometric feature of structural regularity, highlighting the interplay between topological constraints and chemical bonding networks. Numerical analysis of an elliptical helix model indicates that minor perturbations in chemical geometry change do not disrupt this linearity, underscoring the system's structural tolerance. We expect that this study will serve as a valuable perspective for future research in physical-chemistry, where the interplay between molecular geometry, bonding interactions, and energetic stability can be quantitatively explored.

Received 22nd November 2025
Accepted 27th April 2026

DOI: 10.1039/d5ra09032f

rsc.li/rsc-advances

1 Introduction

The canonical double helix structure of deoxyribonucleic acid (DNA), which resembles a spiral staircase, has been investigated since the discovery by Watson and Crick.[1] DNA macromolecules have the primary function of storing genetic information. The double helix is composed of two polynucleotide chains. The single monomeric unit, called a nucleotide, consists of nitrogen containing nucleobases, also called nitrogenous bases (adenine (A), cytosine (C), guanine (G), and thymine (T)), a five-carbon sugar (deoxyribose), and a phosphate group. The nitrogenous bases of the DNA helix store all the genetic information necessary for cellular activity. Hydrogen bonds hold the nitrogenous base pairs together: adenine pairs with thymine (A–T) and guanine pairs with cytosine (G–C). The number of base pairs of the human genome, for instance, is three billion (30×10^8). In the present work, we aim to examine the approximation properties of idealized helical models that underlie many geometric descriptors used in structural chemistry.

The twisting geometry of the double helix results from hydrophilic and hydrophobic interactions between DNA molecules and neighboring water/solvent molecules, temperature, and so on. In recent years, experimental manipulation of the higher order DNA structure through chemical modification has elucidated mechanisms that influence the structural organization of genetic information by regulation of gene expression, nucleic acid therapeutics, nucleic acid medicine, and gene therapy drugs.[2–5] It has also been shown that DNA can be used as a platform for engineered systems that exploit its structural properties in information processing and nanotechnology applications. Those medical and engineering applications indicate that DNA plays a central role not only as individual static genetic memory, but also as a self-assembly function in controlling successive processes.

One might thus wonder whether the twisting double helix structure of DNA is merely one of the results of a variety of chemical interactions without any specific meaning, or, on the contrary, DNA structure exhibits geometric regularities that motivates the question of whether such features can be consistently described within an idealized mathematical framework. Geometric properties of the macromolecular system

[a]*Department of Applied Mathematics, National Sun Yat-sen University, Kaoshiung 80424, Taiwan, Republic of China. E-mail: chenmr@math.nsysu.edu.tw*

[b]*Department of Applied Physics, The University of Osaka, Osaka 565-0871, Japan. E-mail: li7fu@chem.sci.osaka-u.ac.jp*

[c]*Department for the Promotion of Human Science and Quality of Life, Università Telematica San Raffaele, Rome 00166, Italy*

[d]*Department of Chemistry, National Sun Yat-sen University, Kaoshiung 80424, Taiwan, Republic of China*

also relate the stereo-dynamical interactions in a concerted way.[6,7] In this context, the present study employs tools of differential geometry to quantitatively reexamine the relationship between the chemical structures of biomacromolecules and their geometric organization associated with information-carrying molecular structures. We introduce the concept of an action-time parameter, t, and its correlation with the arclength, s, of the canonical double helix to provide a framework for describing the geometric regularity associated with information-carrying molecular structures. Using the Frenet–Serret formulas, we demonstrate the relationship between t and s. This highlights a consistent geometric relationship between molecular structure and curve parametrization.

From a chemical perspective, the geometric invariants of the DNA helix, curvature and torsion, provide a compact description of how stabilizing interactions are distributed along the polymer. In its canonical physiological form (B-DNA), the double helix adopts a right-handed geometry with a highly regular arrangement of base pairs along the molecular axis.[8] Within this structure, hydrogen bonding between complementary bases, π–π stacking among aromatic nucleobases,[9] and electrostatic repulsion between phosphate groups[10] combine to generate a quasi-periodic stabilizing potential. The near constancy of curvature and torsion in the circular helix model reflects this underlying chemical uniformity: on average, each base pair experiences a similar local environment along the axis. From this point of view, the Frenet–Serret framework complements rather than replaces chemical models, offering a mathematically controlled representation of the structural regularity that emerges from collective chemical interactions.

In the present study, we formulate conversion equations between the time parameter t for the information action and the arclength s in the circular helix case (model 1) and the elliptical helix case (model 2). These equations are significant for applying the Frenet–Serret formulas to the geometry of the DNA double helix. Here, we consider the single helix curve instead of the double helix curve, simply because the single helix curve represents the same differential geometry property. We also examine the elliptical helix because the arrangement of five-carbon sugar (deoxyribose) and phosphate groups at both ends of the nucleotide units may somehow deform the double helix structure. The elliptical helix curve function we considered in the present work is as follows:

$$\mathbf{r}(t) = (a\cos t, b\sin t, ct), \quad a, b > 0, c \geq 0 \text{ and } t \in \mathbb{R},$$

where a and b denote the semi-major and semi-minor axes of the underlying elliptic cylinder, and c governs the axial rise per radian. To reduce notational complexity, we set $a = c = 1$. We then compare the two cases and find that for b-values in the range $0.95 \leq b \leq 1.05$, the calculated results closely approximate those obtained at $b = 1$. Therefore, for clarity and without loss of generality, the subsequent study of the Frenet–Serret moving formulas considers only the circular geometry. With the aid of differential geometry, we conclude that the arclength s representation together with the Frenet–Serret moving formulas plays a central role in providing a convenient parametrization of progression, due to the fact that they have the same value for curvature κ and torsion τ. We confirmed the linearity between the arclength s and the action time t in elliptical double-helix geometry.

2 Mathematical formulations

2.1 One-parameter representation of three-dimensional curves

It is convenient to use one parameter t to express a three-dimensional space curve $\mathbf{r}(x, y, z)$, thus it is given as $\mathbf{r}(t)$ with $x(t)$, $y(t)$, $z(t)$. Suppose we imagine the trace of a point's movement along a space curve which results in a trajectory $\mathbf{r}(t)$ so that the parameter t is a notional parameter used to describe progression along the curve, in the present work. It means that we need to introduce "time" in mathematics, while physics describes motion always using the variable "time" t. Mathematics does not require "time" for operations in algebra and geometry. We recall that there is another type of one-parameter representation of a three-dimensional curve $\mathbf{r}$, the arclength s. In the following, we formulate conversion formulas between the two parameters t and s in the circular helix and elliptical helix models, respectively.

2.2 Circular helix model

A circular helix curve aligned along the z-axis provides a canonical example of a spatial curve with the same constant curvature and torsion.[11] Due to its special geometric regularity, it serves as a natural reference model, particularly for the DNA double-helix biopolymers. The helix curve $\mathbf{r}$ can be parameterized using the following equation.

$$\mathbf{r}(t) = (x(t), y(t), z(t)) = (\cos t, \sin t, t), \quad t \in \mathbb{R},$$

Note that at this moment, the curve parameter t should be interpreted purely as a geometric variable rather than as the physical time of motion or information transfer action in the present study. Here, we may use it as a convenient notional parameter without physical interpretation. The corresponding tangent vector at an arbitrary point on the curve

$$\mathbf{v}(t) = \frac{\mathrm{d}\mathbf{r}}{\mathrm{d}t} = (-\sin t, \cos t, 1)$$

is given by the constant norm $\|\mathbf{v}(t)\| = \sqrt{2}$ for the circular helix curve.

Consequently, the arclength $s(t)$, measured from $t = 0$, is given by eqn (1)

$$s(t) = \int_0^t \|\mathbf{v}(u)\| \mathrm{d}u = \int_0^t \sqrt{2} \mathrm{d}u = \sqrt{2}t \tag{1}$$

and the derivative of $s(t)$, denoted by $\mathrm{d}s/\mathrm{d}t$, due to the differential of a composite function, is given below.

$$\frac{\mathrm{d}s}{\mathrm{d}t} = \|\mathbf{v}(u)\| = \sqrt{2}.$$

Therefore, we can confirm that the derivative of $s(t)$ is a constant, establishing a linear relationship between the

arclength s and the curve parameter t. This identity allows us to express all intrinsic geometric quantities, such as curvature and torsion, in the Frenet–Serret equation in terms of s. Consequently, t can be written explicitly in terms of s, eliminating the need for further parameterization. As mentioned, the curve parameter t is typically interpreted as the speed of the representative point moving along the curve.

2.3 Elliptical helix model

As discussed in Subsection 2.2, the circular helix of DNA is a prototypical example of a three-dimensional space curve with the same constant value of curvature and torsion. Suppose that some parts of the DNA macromolecule become somehow anisotropic due to additional chemical bonds, as shown in Fig. 1(a), where the sugar-phosphate backbone exhibits two distinct groove widths. DNA is essentially composed of two helical chains coiled around the same axis with a pitch of 3.4 nm; the pair of chains has a diameter of 2.0 nm and the nucleotide unit is 0.33 nm wide.[12–16] Therefore, the groove width of the sugar-phosphate backbone may cause a slight deviation from the helix curve function. In this subsection, we account for this slight structural deviation using the elliptical helix curve function with the parameter t and the additional constants a, b, and c as given by the following equation.

$$\mathbf{r}(t) = (a\cos t, b\sin t, ct), \quad a, b > 0, c \geq 0 \text{ and } t \in \mathbb{R},$$

where a and b are the semi-major and semi-minor axes of the underlying elliptical cylinder, and c governs the axial rise per radian. To reduce notational complexity and facilitate dimensionless analysis, we set $a = c = 1$. With this normalization, the shape of the helix is determined solely by the parameter b, which characterizes the ellipticity of the cross-section. When $b >$ 1, the semi-major axis lies along the y-axis. In contrast, when $0 <$ $b < 1$, the semi-major axis lies along the x-axis. The case $b = 1$ corresponds to the circular helix. The elliptical helix model, with a suitably wide range of b value, can therefore be interpreted as a reference configuration that enables controlled analysis of deviations from ideal helical symmetry, rather than as a physically realistic representation of chemical modifications in DNA structures observed in experiments or structural databases. The following equation gives the corresponding (unnormalized) tangent vector in the elliptical helix model.

$$\mathbf{v}(t) = (-\sin t,\ b\cos t,\ 1),$$

whose magnitude is given as follows:

$$\|\mathbf{v}(t)\| = \sqrt{\sin^2 t + b^2\cos^2 t + 1} = \sqrt{2 + (b^2 - 1)\cos^2 t}.$$

Like to the circular helix curve function, the b-dependent arclength, $s_b(t)$ measured from $t = 0$ is given by the eqn (2)

$$s_b(t) = \int_0^t \sqrt{2 + (b^2 - 1)\cos^2 u}\,\mathrm{d}u \qquad (2)$$

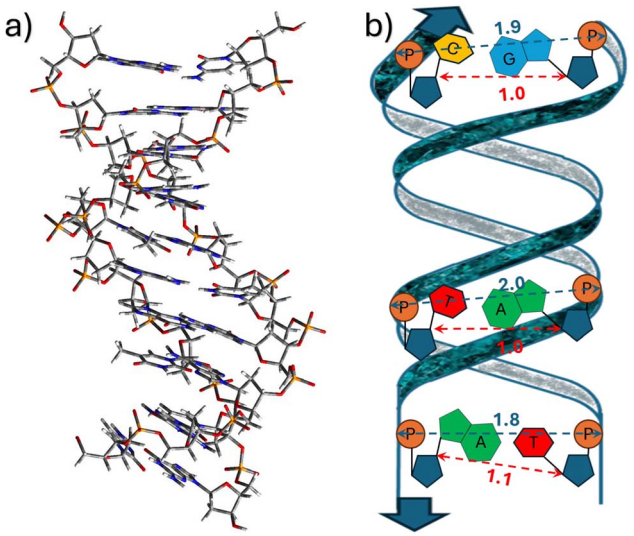

Fig. 1 (a) Structure of DNA (1RN9 from https://www.rcsb.org). (b) Sketch of the double strand of DNA in panel (a) showing the nitrogenous base pairs corresponding to the first, fifth, and tenth nucleotide residues: A–T, T–A, and C–G. The blue pentagon represents deoxyribose, and the orange circle indicates the phosphate group. The blue dashed line with double arrows represents the outer diameter, whose value in nanometers (nm) is indicated by the same color of the line. The outer diameter is determined by the distance between the phosphorus atoms of two symmetric nucleotide units. The inner diameter is indicated by the red dotted line with double arrows. Its value in nm is also shown in red. The inner diameter is given by the distance between the carbon atoms indicated as C_1' of two symmetric nucleotide units. The atom C_1' is the carbon atom of the deoxyribose unit linked to the nitrogenous base.

and the derivative of $s_b(t)$ is given by the equation

$$\frac{\mathrm{d}s_b(t)}{\mathrm{d}t} = \sqrt{2 + (b^2 - 1)\cos^2 t}.$$

For the circular helix, we know that the derivative of the arclength function, $s(t)$, is constant. This yields a linear relationship between the arclength s and the curve parameter t. In contrast, for an elliptical helix, the derivative of the arclength function $s_b(t)$ is no longer constant since

$$\frac{\mathrm{d}s_b(t)}{\mathrm{d}t} = \sqrt{2 + (b^2 - 1)\cos^2 t}$$

explicitly depends on the parameter t. As a result, the arclength s_b does not grow linearly with t, and no closed-form inversion between s_b and t can generally be obtained. This nonlinear relationship between s_b and t complicates the description of intrinsic geometric quantities such as curvature and torsion within the Frenet–Serret framework. Furthermore, since the curve invariants of the elliptical helices usually exhibit periodic behavior, the next subsection presents numerical simulations

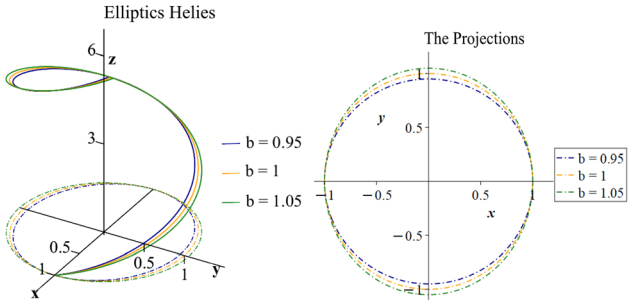

Fig. 2 The left panel shows elliptical helices with $b = 0.95$, 1.00, and 1.05. The solid lines represent the helices, while the dashed lines indicate their planar projections. The right panel presents their planar projections. For $b = 0.95$, the projection is an ellipse with semi-major axis 1 along the x-axis and semi-minor axis 0.95 along the y-axis. For $b = 1.05$, the projection is an ellipse with semi-major axis 1.05 along the y-axis and a semi-minor axis 1 along the x-axis.

examining the values of $s_b(t)$ as a function of b in the range $0.95 \leq b \leq 1.05$.

2.4 Numerical computation and discussion

In Subsection 2.3, we have seen the b-dependent arclength, $s_b(t)$ measured from $t = 0$:

$$s_b(t) = \int_0^t \sqrt{2 + (b^2 - 1)\cos^2 u}\,du.$$

Our analysis shows that the arclength s_b does not increase linearly with t. In other words, the derivative of s_b explicitly depends on t. This nonlinearity contrasts with the special case $b = 1$, which corresponds to the circular helix, in which the growth of the arclength $s_1(t)$ is strictly proportional to t (Fig. 2).

Closed-form expressions involving complete elliptic integrals are available only for $b = 1$, which corresponds to the circular helix. For general values of b, however, the arclength function $s_b(t)$ does not admit an analytical form and must be evaluated numerically. In this study, we use Maple to compute $s_b(t)$ *via* standard numerical integration techniques. Suitable methods include Romberg integration and adaptive quadrature algorithms, such as those implemented in the QUADPACK library.[17,18]

We consider deviations of up to ±5% from helical geometry, as a representative small-perturbation range for assessing the sensitivity of the geometric invariants. This range is also comparable in magnitude to variations associated with the groove width of the DNA sugar-phosphate backbone. Since $\cos t$ is periodic with a period of 2π and the elliptical helix is symmetric about the x-axis, the arclength at $t = n\pi$ (where n is an integer) is n times the arclength over $[0, \pi]$. Table 1 reports the computed values of the arclength $s_b(\pi)$ for selected values of b in the range $0.95 \leq b \leq 1.05$. The dependence of $s_b(\pi)$ on b is illustrated in Fig. 3. As b increases, both the arclength and the ratio $s_b(\pi)/s_1(\pi)$ increase monotonically.

From this periodicity, it follows that

Table 1 Arclength $s_b(\pi)$ of the elliptical helix as a function of the y-axis semi-radius b, with normalized ratios relative to the circular case ($b = 1$). As b increases, both the arclength and the ratio $s_b(\pi)/s_1(\pi)$ increase monotonically

y-Axis semi-radius b	Arclength $s_b(\pi)$	Ratio $s_b(\pi)/s_1(\pi)$
0.95	4.388	0.988
0.96	4.399	0.990
0.97	4.410	0.993
0.98	4.421	0.995
0.99	4.432	0.998
1.00	4.443	1.000
1.01	4.454	1.002
1.02	4.465	1.005
1.03	4.477	1.008
1.04	4.488	1.010
1.05	4.499	1.013

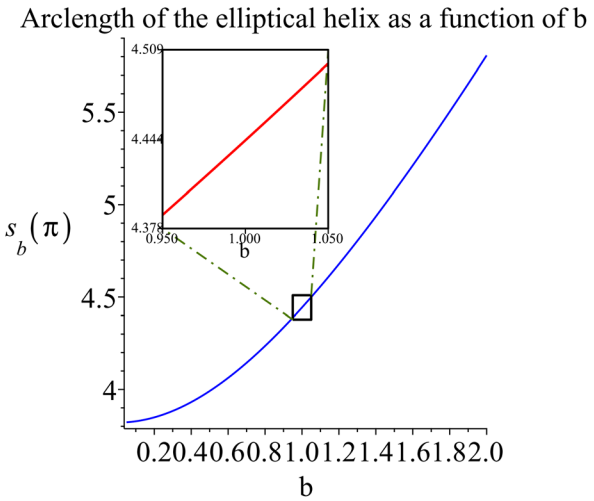

Fig. 3 Arclength of the elliptical helix as a function of b. Within the examined range, the dependence is nearly linear, indicating that small variations in ellipticity produce proportional changes in helix length.

$$s_b(n\pi) = n\int_0^{\pi} \sqrt{2 + (b^2 - 1)\cos^2 u}\,du.$$

Consequently, the long-term mean arclength growth rate, denoted μ_b, is obtained from the limit of $s_b(t)/t$. That is,

$$\frac{s_b(t)}{t} \to \mu_b = \frac{1}{\pi}\int_0^{\pi} \sqrt{2 + (b^2 - 1)\cos^2 u}\,du, \quad \text{as } t \to \infty. \qquad (3)$$

This limit shows that μ_b quantifies the asymptotic arclength increment per unit change in the parameter t. Equivalently, for large t (for example: $t > 28\pi$),

$$s_b(t) \sim \mu_b t.$$

Table 2 Asymptotic arclength growth rate μ_b of the elliptical helix as a function of the y-axis semi-radius b, with normalized ratios relative to the circular case ($b = 1$)

y-Axis semi-radius b	Growth rate μ	Ratio μ_{bb}/μ_1
0.95	1.3968	0.988
0.96	1.4003	0.991
0.97	1.4037	0.993
0.98	1.4072	0.995
0.99	1.4107	0.998
1.00	1.4142	1.000
1.01	1.4178	1.003
1.02	1.4213	1.005
1.03	1.4249	1.008
1.04	1.4285	1.010
1.05	1.4322	1.013

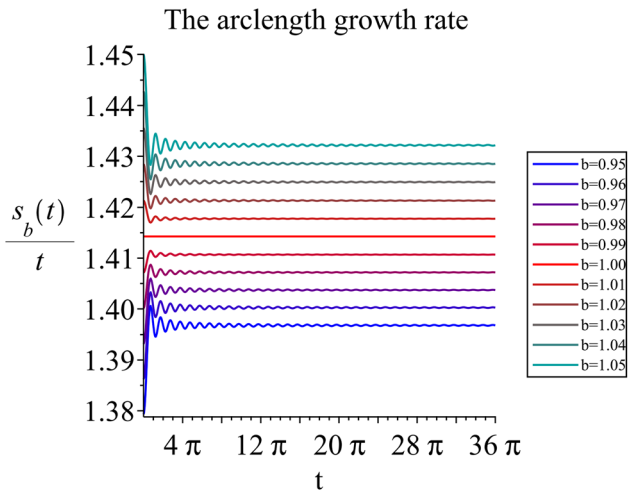

Fig. 4 Graphical representation of the arclength growth rate $s_b(t)/t$ as a function of the y-axis semi-radius b. Larger b yields larger $s_b(t)/t$, and hence larger μ_b.

Table 2 lists the values of μ_b for representative b in the range $0.95 \leq b \leq 1.05$, while Fig. 4 displays the arclength growth rate $s_b(t)/t$. As t grows, this ratio stabilizes at a constant μ_b for each b. A larger b corresponds to a larger μ_b. Moreover, eqn (3) yields

$$\frac{t}{s_b(t)} \to \frac{1}{\mu_b},$$

so that $1/\mu_b$ represents the asymptotic axial rise per full 2π revolution of the curve.

In molecular terms, this relation provides a practical correspondence between the contour length and axial displacement for a polymer constrained to an elliptical–helical scaffold: local torsional fluctuations do not affect the asymptotic drift $1/\mu_b$.

3 Frenet–Serret formulas

The geometric evolution of any nonlinear curve in the three-dimensional Euclidean space is governed by the Frenet–Serret equations:[19]

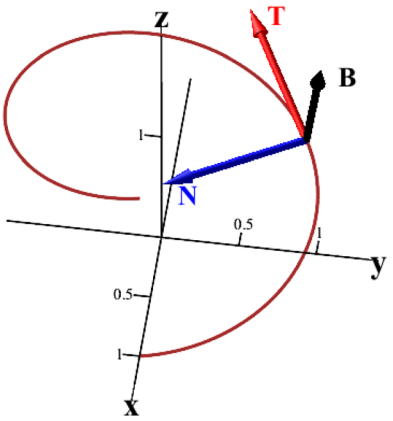

Fig. 5 Three orthonormal coordinate vectors along the curve: tangent vector **T**, normal vector **N**, and binormal vector **B**. The parameter s represents arclength, while κ and τ denote the curvature and torsion of the curve, respectively.

$$\begin{aligned} \frac{d\mathbf{T}}{ds} &= \kappa\mathbf{N}, \\ \frac{d\mathbf{N}}{ds} &= -\kappa\mathbf{T} + \tau\mathbf{B}, \\ \frac{d\mathbf{B}}{ds} &= -\tau\mathbf{N}. \end{aligned} \tag{4}$$

These equations describe the orthonormal moving frame $\{\mathbf{T}, \mathbf{N}, \mathbf{B}\}$ along the spatial trajectory as a function of arclength s, namely $\mathbf{r}(s)$. This provides a complete local geometric characterization through the curvature of scalar invariants κ and torsion τ. As shown in Fig. 5, the tangent vector **T** indicates the instantaneous direction of motion. The normal vector **N** points to the center of curvature, and the binormal vector $\mathbf{B} = \mathbf{T} \times \mathbf{N}$ completes a right-handed orthonormal triad. Together with the position vector $\mathbf{r}(s)$, this moving frame constitutes the classical Frenet–Serret frame, which is a fundamental tool in differential geometry and molecular conformational analysis, including that of the circular and elliptical DNA helix.

3.1 Frenet–Serret formula for circular helix model

For Section 2.2 and the linear relationship $s(t) = \sqrt{2}t$, the circular helical curve can be reparametrized in terms of arclength as follows

$$\mathbf{r}(s) = \left(\cos\frac{s}{\sqrt{2}}, \sin\frac{s}{\sqrt{2}}, \frac{s}{\sqrt{2}}\right).$$

The corresponding unit tangent vector of the circular helix is given as follows.

$$\mathbf{T}(s) = \frac{d\mathbf{r}(s)}{ds} = \left(-\frac{1}{\sqrt{2}}\sin\frac{s}{\sqrt{2}}, \frac{1}{\sqrt{2}}\cos\frac{s}{\sqrt{2}}, \frac{1}{\sqrt{2}}\right).$$

Differentiating $\mathbf{T}(s)$ with respect to s and normalizing yields the unit normal vector,

$$\mathbf{N}(s) = \frac{\mathrm{d}\mathbf{T}(s)/\mathrm{d}s}{\|\mathrm{d}\mathbf{T}(s)/\mathrm{d}s\|} = \left(-\frac{1}{\sqrt{2}}\cos\frac{s}{\sqrt{2}}, \frac{1}{\sqrt{2}}\sin\frac{s}{\sqrt{2}}, 0\right),$$

and the unit binormal vector is given by

$$\mathbf{B}(s) = \mathbf{T}(s) \times \mathbf{N}(s) = \left(\frac{1}{\sqrt{2}}\sin\frac{s}{\sqrt{2}}, -\frac{1}{\sqrt{2}}\cos\frac{s}{\sqrt{2}}, \frac{1}{\sqrt{2}}\right).$$

The curvature and torsion of the curve are calculated as

$$\kappa(s) = \|\frac{\mathrm{d}\mathbf{T}(s)}{\mathrm{d}s}\| = \frac{1}{\sqrt{2}},$$

$$\tau(s) = -\frac{\mathrm{d}\mathbf{B}(s)}{\mathrm{d}s}\cdot\mathbf{N}(s) = \frac{1}{\sqrt{2}},$$

and hence the ratio $\kappa(s)/\tau(s) = 1$, which characterizes a uniform helix geometry. Furthermore, using eqn (4), the Frenet–Serret equations are as follows.

$$\frac{\mathrm{d}\mathbf{T}(s)}{\mathrm{d}s} = \frac{1}{\sqrt{2}}\mathbf{N}(s),$$

$$\frac{\mathrm{d}\mathbf{N}(\mathbf{s})}{\mathrm{d}s} = -\frac{1}{\sqrt{2}}\mathbf{T}(s) + \frac{1}{\sqrt{2}}\mathbf{B}(s),$$

$$\frac{\mathrm{d}\mathbf{B}(s)}{\mathrm{d}s} = -\frac{1}{\sqrt{2}}\mathbf{N}(\mathbf{s}).$$

Using the Frenet–Serret frame to analyze the DNA double helix provides direct geometric insight into its structural regularity. For an ideal DNA helix, the arclength s is linearly related to the helical angular parameter t *via* $s(t) = \sqrt{2}t$. This implies a uniform helical progression with constant curvature and torsion. This relationship enables the arclength to serve as an affine surrogate for progression along the DNA molecular axis. Furthermore, the constant curvature and torsion imply that the local conformational geometry remains invariant along the helix. This is consistent with the view that, within an idealized helix model, base-pair positions can be described within a homogeneous geometric scaffold. Thus, this geometric framework provides a controlled representation of helical regularity and can be used to assess the robustness of curvature- and torsion-based descriptors under small perturbations.

3.2 Frenet–Serret formula for elliptical helix models

To obtain the Frenet–Serret formulas for elliptical helices using eqn (4), we first need to calculate their arclength. As noted above, there are no closed formulas available for this arclength. Therefore, we use t as a parameter to compute the curvature κ and torsion τ of an elliptical helix and derive the corresponding Frenet–Serret formulas.

Let $\mathbf{r}(t)$ be defined as in Subsection 2.3 with $a = 1 = c$. That is,

$$\mathbf{r}(t) = (\cos t, b\sin t, t), \quad b > 0 \text{ and } t \in \mathbb{R}.$$

From the definition of curvature and torsion,[19] curvature and torsion are functions of the variable b, and we have the following expression.

$$\kappa_b(t) = \frac{\|\mathbf{r}' \times \mathbf{r}''\|}{\|\mathbf{r}'\|^3} = \sqrt{\frac{2b^2 - (b^2-1)\cos^2 t}{\left[2 + (b^2-1)\cos^2 t\right]^3}}, \tag{5}$$

$$\tau_b(t) = \frac{(\mathbf{r}' \times \mathbf{r}'')\cdot\mathbf{r}'''}{\|\mathbf{r}' \times \mathbf{r}''\|^2} = \frac{b}{2b^2 - (b^2-1)\cos(t)^2}. \tag{6}$$

From the above expressions, we see that the curvature $\kappa_b(t)$ and torsion $\tau_b(t)$ are not constants except when $b = 1$ (for the circular case). In fact, the curvature $\kappa_1(t) = 1/2$ and the torsion $\tau_1(t) = 1/2$ are equal to 1/2 for the circular helices. We also find that the ratio $\kappa_b(t)/\tau_b(t)$ is not equal to one unless $b = 1$ (the circular case). Specifically, this ratio is given as follows:

$$\frac{\kappa_b(t)}{\tau_b(t)} = b\left(\frac{2b^2 - (b^2-1)\cos^2 t}{2 + (b^2-1)\cos^2 t}\right)^{2/3} \neq 1 = \frac{\kappa_1(t)}{\tau_1(t)}.$$

The Frenet–Serret formulas for an elliptical helix model are as follows:

$$\frac{\mathrm{d}\mathbf{T}(t)}{\mathrm{d}t} = \|\mathbf{v}(t)\|\kappa_b(t)\mathbf{N}(t),$$

$$\frac{\mathrm{d}\mathbf{N}(t)}{\mathrm{d}t} = -\|\mathbf{v}(t)\|(\kappa_b(t)\mathbf{T}(t) + \tau_b(t)\mathbf{B}(t)),$$

$$\frac{\mathrm{d}\mathbf{B}(t)}{\mathrm{d}t} = \|\mathbf{v}(t)\|\tau_b(t)\mathbf{N}(t).$$

By substituting the expressions for curvature and torsion into the above equations, we obtain the following complicated formulas:

$$\frac{\mathrm{d}\mathbf{T}(t)}{\mathrm{d}t} = \frac{\sqrt{2b^2 - (b^2-1)\cos^2 t}}{2 + (b^2-1)\cos^2 t}\mathbf{N}(t),$$

$$\frac{\mathrm{d}\mathbf{N}(t)}{\mathrm{d}t} = -\frac{\sqrt{2b^2 - (b^2-1)\cos^2 t}}{2 + (b^2-1)\cos^2 t}\mathbf{T}(t)$$

$$+\frac{b\sqrt{2 + (b^2-1)\cos^2 t}}{2b^2 - (b^2-1)\cos^2 t}\mathbf{B}(t), \quad \frac{\mathrm{d}\mathbf{B}(t)}{\mathrm{d}t} = \frac{b\sqrt{2 + (b^2-1)\cos^2 t}}{2b^2 - (b^2-1)\cos^2 t}\mathbf{N}(t).$$

We used Maple to calculate the curvature $\kappa_b(t)$ and torsion $\tau_b(t)$ for selected values of b in the range $0.95 \leq b \leq 1.05$, considering deviations up to 5% from the standard helical geometry, as presented in Tables 3 and 4, which are provided in Appendix A. Fig. 6 illustrates the dependence of $\kappa_b(t)$ and $\tau_b(t)$ on b. Eqn (5) and (6), show that both $\kappa_b(t)$ and $\tau_b(t)$ are periodic functions due to their dependence on $\cos t$. This is also reflected in Fig. 6, which is also provided in the Appendix B. Conse-

quently, Tables 3 and 4 only report the values of $\kappa_b(t)$ and $\tau_b(t)$ over the interval $t \in [0, \pi/2]$. Additionally, in Tables 3 and 4, the values (ratios) in red indicate the maximum, while the values in blue indicate the minimum. The maximum ratio ($\kappa_b(t)/\kappa_1(t)$ or $\tau_b(t)/\tau_1(t)$) is approximately 1.05, and the minimum is approximately 0.95.

4 Discussions and conclusions

In this work, we employed mathematical tools to confirm that applying the Frenet–Serret moving frame to the DNA double helix provides not only a mathematical description of its geometry but also a geometric grounded perspective on its structural regularity. For the circular DNA helix, the arclength s is linearly related to the helical angular parameter t *via* the relation $s(t) = \sqrt{2}t$, indicating uniform helical progression with constant curvature and torsion. This correspondence allows the arclength s to serve as an affine surrogate for the progression along the molecular axis. Furthermore, the constant curvature and torsion imply that the local conformational geometry is invariant along the helix. This reinforces the idea that base-pair positions can be described using the linear parameter t within a globally homogeneous geometric framework. The invariance of curvature and torsion is consistent with the high degree of structural regularity observed in DNA helices, where hydrogen bonding between complementary bases, π–π stacking interactions among aromatic nucleobases, and electrostatic repulsion between phosphate groups are typically distributed in a quasi-periodic manner along the molecular axis. This uniformity is associated with a reduced variation of local geometric descriptors along the model helix. The uniform parameter s provides a convenient parametrization for describing uniform progression along the idealized helical geometry. This geometric framework provides a consistent representation of helical regularity and highlights the robustness of curvature- and torsion-based descriptors used to characterize DNA structure. Accordingly, we have presented the mathematical interpretation of how the double-helix geometry can be consistently described within an idealized geometric framework. This provides a consistent geometric framework for describing base-pair organization within an idealized helical model. Although the exact chemical bond of DNA is complex, the numerical results of the elliptical helix model indicate that when b falls within the range of $0.95 \leq b \leq 1.05$, the system can be effectively treated as a circular helix.

To place these geometric deviations in a chemical context, it is useful to compare them with the canonical structural parameters of B-DNA. In its physiological form, B-DNA adopts a right-handed double helix with a diameter of approximately 2.0 nm, a helical pitch of about 3.4 nm, and roughly 10–10.5 base pairs per helical turn.[8] These values reflect the quasi-periodic distribution of stabilizing interactions along the polymer, including hydrogen bonding between complementary bases, π–π stacking among aromatic nucleobases, and electrostatic repulsion between phosphate groups.[10] Within this framework, a ±5% variation in cross-sectional ellipticity corresponds to geometric perturbations comparable in magnitude to those induced by common local chemical modifications, such as methylation or oxidative lesions. The numerical results obtained for the elliptical helix model thus provide a quantitative estimate of the tolerance of the DNA scaffold to chemically induced distortions, and support the use of the circular helix as a robust reference geometry in structural and physico-chemical analyses.

This reinforces the idea that base-pair positioning can be described within a globally homogeneous structural ensemble. The stability of this geometry is further supported by the cooperative nature of hydrogen bonds and stacking forces, which absorb small perturbations without significantly altering the overall geometric characteristics. This geometric framework supports a consistent molecular mechanism for base-pair interactions and highlights the architectural efficiency of DNA as a geometrically robust framework for organizing genetic information. We expect that this study will serve as a valuable perspective for future research in physical-chemistry, where the interplay between molecular geometry, bonding interactions, and energetic stability can be quantitatively explored. By framing the DNA double helix within a geometric physical model, our results highlight how curvature and torsion translate into stability against chemical perturbations and efficiency in information transfer. This physico-chemical viewpoint opens pathways to investigate DNA not only as a carrier of genetic code but also as a paradigmatic system for understanding how structure governs function in complex biomacromolecules.

Conflicts of interest

There are no conflicts to declare.

Data availability

All data supporting the findings of this study were generated directly by the authors using Maple 2024.1 with standard built-in functions. No external databases or thirdparty datasets were used, and no custom algorithms were developed. All computations can be reproduced based on the methodological descriptions provided in the manuscript. The Maple scripts and datasets that support this work are openly available on GitHub and archived in Zenodo at DOI: [https://doi.org/10.5281/zenodo.17559225]. The repository includes the Maple 2024.1 source script, example input/output data, and detailed instructions for reproduction.

Appendices

Appendix A

Table 3 Simulation values of the curvature $\kappa_b(t)$ for different curve parameter t and the y-axis semi-radius b. Each entry shows $\kappa_b(t)$ (top) and the normalized ratio $\kappa_b(t)/\kappa_1(t)$ (bottom). Values in red indicate the maximum, while values in blue indicate the minimum

	The y-axis semi-radius b										
The parameter t	0.95	0.96	0.97	0.98	0.99	1.00	1.01	1.02	1.03	1.04	1.05
0	0.526 (1.052)	0.520 (1.040)	0.515 (1.030)	0.510 (1.020)	0.505 (1.010)	0.500 (1.000)	0.495 (0.990)	0.490 (0.980)	0.485 (0.970)	0.480 (0.960)	0.476 (0.952)
$\pi/8$	0.518 (1.036)	0.514 (1.028)	0.511 (1.022)	0.507 (1.014)	0.504 (1.008)	0.500 (1.000)	0.496 (0.992)	0.493 (0.986)	0.489 (0.978)	0.486 (0.972)	0.482 (0.964)
$\pi/4$	0.500 (1.000)	0.500 (1.000)	0.500 (1.000)	0.500 (1.000)	0.500 (1.000)	0.500 (1.000)	0.500 (1.000)	0.500 (1.000)	0.500 (1.000)	0.500 (1.000)	0.500 (1.000)
$3\pi/8$	0.482 (0.964)	0.486 (0.972)	0.489 (0.978)	0.493 (0.986)	0.496 (0.992)	0.500 (1.000)	0.504 (1.008)	0.507 (1.014)	0.510 (1.020)	0.514 (1.028)	0.517 (1.034)
$\pi/2$	0.475 (0.950)	0.480 (0.960)	0.485 (0.970)	0.490 (0.980)	0.495 (0.990)	0.500 (1.000)	0.505 (1.010)	0.510 (1.020)	0.515 (1.030)	0.520 (1.040)	0.525 (1.050)

Table 4 Simulation values of the torsion $\tau_b(t)$ for different curve parameter t and the y-axis semi-radius b. Each entry shows $\tau_b(t)$ (top) and the normalized ratio $\tau_b(t)/\tau_1(t)$ (bottom). Values in red indicate the maximum, while values in blue indicate the minimum

	The y-axis semi-radius b										
The parameter t	0.95	0.96	0.97	0.98	0.99	1.00	1.01	1.02	1.03	1.04	1.05
0	0.499 (0.998)	0.500 (1.000)	0.500 (1.000)	0.500 (1.000)	0.500 (1.000)	0.500 (1.000)	0.500 (1.000)	0.500 (1.000)	0.500 (1.000)	0.500 (1.000)	0.499 (0.998)
$\pi/8$	0.503 (1.006)	0.503 (1.005)	0.502 (1.004)	0.501 (1.003)	0.501 (1.001)	0.500 (1.000)	0.499 (0.999)	0.498 (0.997)	0.498 (0.995)	0.497 (0.994)	0.496 (0.992)
$\pi/4$	0.512 (1.025)	0.510 (1.020)	0.507 (1.015)	0.505 (1.010)	0.502 (1.005)	0.500 (1.000)	0.498 (0.995)	0.495 (0.990)	0.493 (0.985)	0.490 (0.980)	0.488 (0.975)
$3\pi/8$	0.522 (1.044)	0.518 (1.036)	0.513 (1.026)	0.509 (1.018)	0.504 (1.009)	0.500 (1.000)	0.496 (0.991)	0.492 (0.984)	0.487 (0.975)	0.483 (0.967)	0.479 (0.959)
$\pi/2$	0.526 (1.053)	0.521 (1.042)	0.515 (1.031)	0.510 (1.020)	0.505 (1.010)	0.500 (1.000)	0.495 (0.990)	0.490 (0.980)	0.485 (0.971)	0.481 (0.962)	0.476 (0.952)

Appendix B

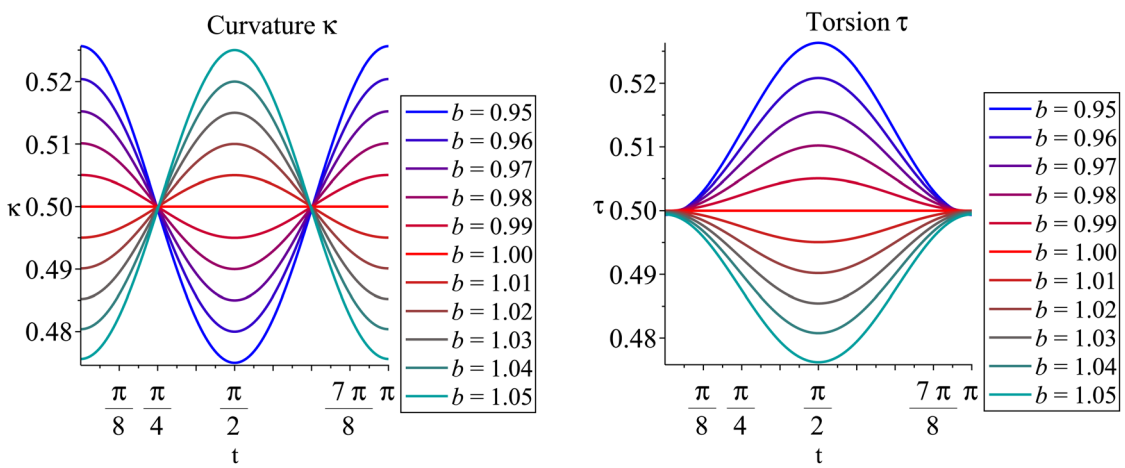

Fig. 6 The left figure shows the curvature κ and the right figure shows the torsion τ. Both curvature κ and torsion τ of the elliptical helix are functions of t for different values of b. Deviations of b from unity increase the oscillatory amplitudes of both κ and τ, while keeping the mean values close to 0.5, which reflects the sensitivity of helical geometry to ellipticity.

Acknowledgements

MC acknowledges financial support from the National Science and Technology Council (NSTC), Taiwan. TK thanks Prof. Shinichi Kotani, Osaka University, Prof. Taku Onishi, Mie University, Japan, and Prof. Po-Yu Tsai of National Chung Hsing University, Taiwan, for their productive discussions. He cordially appreciates Prof. Jyh-Tung Lee (the dean of the College of Science) and Prof. Chunhu Chen, National Sun Yat-sen University, Taiwan, for their financial support to make this study possible.

References

1 J. D. Watson and F. H. C. Crick, *Nature*, 1953, **171**, 737–738.
2 S. Sasaki and H. Murase, *Drug Delivery Syst.*, 2024, **39**, 53–62.
3 N. Sugimoto, T. Endoh, S. Takahashi and H. Tateishi-Karimata, *Bull. Chem. Soc. Jpn.*, 2021, **94**, 1970–1998.
4 K. D. Makova and M. H. Weissensteiner, *Trends Genet.*, 2023, **39**, 109–124.
5 M. T. Banco and A. R. Ferré-D'Amaré, *RNA*, 2021, **27**, 390–402.
6 T. Kasai and K.-C. Lin, *J. Chin. Chem. Soc.*, 2017, **64**, 25–32.
7 T. Kasai, K.-C. Lin, P.-Y. Tsai, M. Nakamura, D.-C. Che, F. Palazzetti and B. Muthiah, *Quantum Science: the Frontier of Physics and Chemistry*, Springer, Singapore, 2022, pp. 67–156.
8 W. Saenger, *Principles of Nucleic Acid Structure*, Springer, New York, 1984.
9 P. Yakovchuk, E. Protozanova and M. D. Frank-Kamenetskii, *Nucleic Acids Res.*, 2006, **34**, 564–574.
10 V. A. Bloomfield, D. M. Crothers and I. Tinoco Jr, *Nucleic Acids: Structures, Properties, and Functions*, University Science Books, Sausalito, 2000.
11 A. H. Louie, R. L. Somorjai and A. Klug, *J. Mol. Biol.*, 1983, **168**, 143–162.
12 S. Amnuanpol, *J. Biol. Phys.*, 2016, **42**, 69–82.
13 R. Hardison, 2.5: B-Form, A-Form, and Z-Form of DNA, https://bio.libretexts.org/Bookshelves/Genetics/Working_with_Molecular_Genetics_(Hardison)/Unit_I:_Genes_Nucleic_Acids_Genomes_and_Chromosomes/2:_Structures_of_Nucleic_Acids/2.5:_B-Form_A-Form_and_Z-Form_of_DNA, Accessed August 15, 2025.
14 J. Mou, D. M. Czajkowsky, Y. Zhang and Z. Shao, *FEBS Lett.*, 1995, **371**, 279–282.
15 V. V. Rybenkov, N. R. Cozzarelli and A. V. Vologodskii, *Proc. Natl. Acad. Sci. U. S. A.*, 1993, **90**, 5307–5311.
16 L. Wang, N. Lu, S. Huang, M. Wang, X.-M. Chen and H. Yang, *CCS Chem.*, 2021, **3**, 1787–1796.
17 R. Piessens, E. De Doncker-Kapenga, C. W. Überhuber and D. K. Kahaner, *Quadpack: A Subroutine Package for Automatic Integration*, Springer, Berlin, 1983.
18 W. Romberg, *Norske Vid. Selsk. Forh., Trondheim*, 1955, **28**, 30–36.
19 B. O'Neill, *Elementary Differential Geometry*, Academic Press, San Diego, 1997.